DE G

Fractional Calculus & Applied Analysis
An International Journal for Theory and Applications
VOLUME 22, NUMBER 5 (2019)
(Print) ISSN 1311-0454
(Electronic) ISSN 1314-2224

SURVEY PAPER

SIMPLIFIED FRACTIONAL-ORDER DESIGN OF A MIMO ROBUST CONTROLLER

Patrick Lanusse [1], **Massinissa Tari** [2]

Abstract

This paper presents how to design as simply as possible a robust MIMO controller for a refrigeration system with a 2 inputs, 2 outputs and a non-linear model. Even if the proposed method starts from the CRONE MIMO approach, the analysis of the linear MIMO behavior of the system model shows that its MIMO controller can be decentralized and designed in two simple steps based on the SISO CRONE methodology. Simulation results show the good control performance and robust stability for a wide set of operating points.

MSC 2010: Primary 93B51; Secondary 26A33, 37N40, 49N35, 70Q05, 93B35, 93B52, 93C35, 93C80, 93D09

Key Words and Phrases: refrigeration systems; robust control; MIMO system; CRONE control design; fractional order PID

Editorial Note: This paper is based on an invited talk at "ICFDA 18" (International Conference on Fractional Differentiation and Applications, 16-18 July 2018, Amman - Jordan). But the manuscript was delayed after the SI related to ICFDA 18 was already completed and published in FCAA, Vol. 22, No 1 (2019).

1. Introduction

Many Control-System Design (CSD) methodologies are proposed for the design of fractional order controllers [22], [13], [25]. The CSD CRONE

pp. 1177–1202 , DOI: 10.1515/fca-2019-0063 DE GRUYTER

methodology is a frequency-domain approach developed since the eighties [15], [16], [20] in order to design robust feedback controller by taking into account the perturbed linear model of a plant. The control-system is based on the common unity-feedback configuration and the principle of the CRONE control methodology is to tune a small number of parameters of fractional order transfer functions which define the feedback controllers. For instance, for the third generation of the SISO CRONE methodology, the nominal open-loop transfer function is defined by using band-limited complex fractional order integrations [7], it is tuned by taking into account closed loop robustness and performance constraints, then the rational transfer function of the controller is synthesized in order to achieve the nominal open-loop frequency response that have been optimized.

For MIMO systems, when the analysis of the plant model shows strong coupling effects the controller transfer function and design should be fully MIMO. Sometimes, the controller could be decentralized and designed either with the full MIMO CRONE methodology or simply by a multi-SISO CRONE methodology that take into account explicitly the MIMO behavior of the plant. Such a Multi-SISO approach could be used to design decentralized MIMO controllers with other fractional order CSD methodologies.

Section 2 presents briefly the roots of the current CRONE design methodology. Section 3 deals with MIMO systems and explains how the plant behavior can be analyzed to determine if a decentralized controller could be high-performing and if the multi-SISO CRONE design could be used. The application to the refrigeration system is presented by Section 4. The CRONE SISO toolbox [10] will be used.

2. Developments of the CRONE control design methodology

2.1. Roots of the CRONE control design methodologies.

Based on the unity-feedback configuration (Fig. 1), the objective of all CRONE CSD methodologies have always been to robustify the closed loop dynamic performance through a robust stability degree (robust resonant peak) and performance.

$G(s)$ is the Linear Time Invariant (LTI) perturbed plant model and $C(s)$ its linear controller. $D_u(s)$ and $D_y(s)$ are disturbances on input and output. $N_m(s)$ is a measurement noise and $U(s)$ is the control effort. $Y(s)$ is the actual plant output and $Y_{ref}(s)$ its set point. The open-loop gain crossover frequency is named ω_{cg}.

In 1975, [15] designed an analog electronic system with a 3/2 fractional order integrator to control a laser frequency with a reduced sensitivity to temperature, pressure, cavity and amplification cell vibration, dye inhomogeneity and turbulence. Using an order 1/2 differentiator, Oustaloup

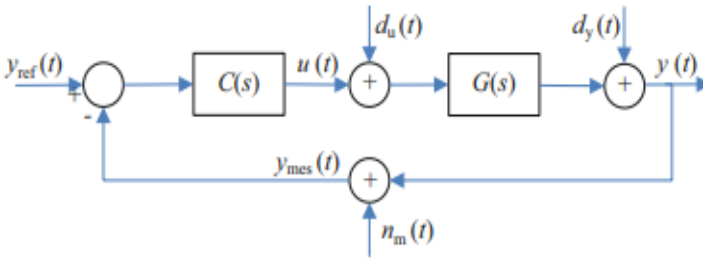

FIGURE 1. Unity-feedback control configuration

proposed in 1979 a PLL frequency demodulator (Fig. 2) whose stability degree was desensitized to the reference signal input and the reception level. These two applications were achieved thanks to the famous Oustaloup's approximation technique which permits a band limited fractional order n transfer function to be replaced by a low order rational transfer function with an equal number of zeros and poles defined by recursive ratios α end η, [21]:

$$C_F(s) = C_0 \left(\frac{1 + \frac{s}{\omega_1}}{1 + \frac{s}{\omega_h}} \right)^n \rightarrow C_R(s) = C_0 \prod_{i=1}^{N} \frac{1 + \frac{s}{\omega_i'}}{1 + \frac{s}{\omega_i}} \tag{2.1}$$

with $n = \frac{log\alpha}{\alpha\eta}, \omega_{i+1}' = \alpha\eta\omega_i'$ and $\omega_i = \alpha\omega_i'$.

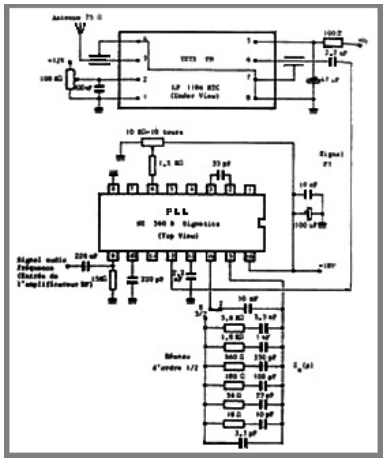

FIGURE 2. PLL frequency demodulator

In 1987, the control of a Saffron picker wire-guided mobile robot has been studied. The saddle cart with driving wheels at the rear, was guided

by a an electromagnetic signal emitted at the rear, received and reemitted by a wire buried in the middle of each row, received by 2 coils in the front. The gain between the cart position and the received signal was weakly known and nonlinear. Thus a robust controller has been designed from the rational approximation of a fractional order nominal open-loop transfer function:

$$\beta_F(s) = \left(\frac{\omega_{cg}}{s}\right)^n \rightarrow \beta_R(s) = \beta_0 \prod_{i=1}^{N} \frac{1+\frac{s}{\omega_i'}}{1+\frac{s}{\omega_i}} \rightarrow C(s) = \frac{\beta_R(s)}{G_{nom}(s)}. \tag{2.2}$$

For cutting machine of Lectra company [16], it has been used for the control of the XY displacement of various cutting tools (laser, high pressure water, knife) for several kinds of fabric (leather, cloth, airbag) (Fig. 3).

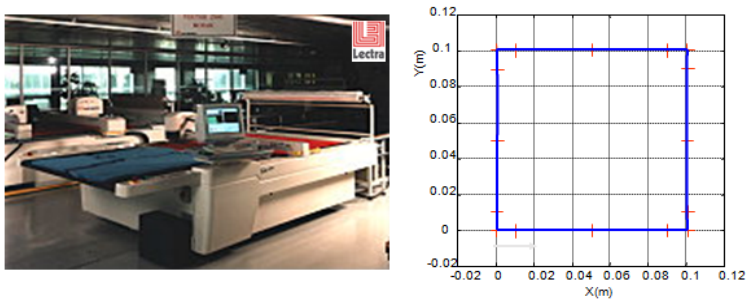

FIGURE 3. Cutting machine of Lectra company, and high speed displacement obtained using a CRONE controller

For gain uncertain plants whose linear models also exhibit frequency-dependent phases, [17] proposed to synthesize a narrow band fractional order open-loop transfer function by using a complex order band limited differentiator:

$$C_F(s) = C_0 \left(\frac{1+\frac{s}{\omega_1}}{1+\frac{s}{\omega_h}}\right)_{C_j}^{a+ib} \rightarrow C_R(s) = C_0 \prod_{i=1}^{N} \frac{1+\frac{s}{\omega_k'}}{1+\frac{s}{\omega_k}} \rightarrow \beta(j\omega) = \left(\frac{\omega_{cg}}{j\omega}\right)^n. \tag{2.3}$$

Oustaloup et al., first for plants with large gain variations [18], then for plants with both gain and phase uncertainties [19], proposed to design robust controllers using a final frequency-domain approximation of controllers:

$$\beta_F(s) = \left(\frac{\omega_{cg}}{s}\right)_{C_j}^{a+ib} \rightarrow C_R(j\omega) = \frac{\beta_F(j\omega)}{G_{nom}(j\omega)} \rightarrow C_R(s). \tag{2.4}$$

For Massey-Ferguson company, it has been apply to a tractor electro-hydraulic hitch-system [5] for the robust control of the tool working depth,

while limiting the slip rate by taking into account. The controller needed to be robust with respect to the working depth and the kind of tool, the non-homogeneity and soil type, the nonlinear static and dynamic model (Fig. 4).

Thus, the 3^{rd} generations of the SISO CRONE CSD have been defined and named [6], [7]. Each generation extends the application field of the CRONE methodology while trying to keep simple the robust controller design. The 1^{st} generation is for gain-like plant perturbation model and for constant plant phase around ω_{cg}. The controller is defined as a common filtered PID cascade controller but with a real fractional order derivative term. The 2^{nd} generation is for gain-like plant perturbation model with frequency-dependent phase. The nominal open-loop transfer function is defined from a real fractional order integrator around ω_{cg}. For most general perturbation models, the 3^{rd} generation uses a nominal open-loop transfer function defined from a complex fractional order integrator. The resonant frequency (bandwidth) and peak M_{rd} (stability degree) of the complementary sensitivity transfer function are specified for the nominal model of the plant. Taking into account the plant perturbation model (defined without any overestimation), only 3 high-level and independent open-loop parameters are optimized in order to minimize the variations of the resonant peak while the 4 common sensitivity functions meet specification defined by 5 frequency-domain constraints.

FIGURE 4. Robust design of an open-loop Nyquist locus for the control of working depth and slip rate related to a tractor three point hitch

2.2. **Simplifications of the SISO 3^{rd} CRONE control methodology.** Because a given choice of the nominal bandwidth is not obvious, the nominal open-loop gain crossover frequency ω_{cg} or closed-loop resonant frequency ω_r (whose set the nominal bandwidth closed-loop dynamics) became

early an optimized parameter in order to adapt the bandwidth to the reachable control-effort level, to avoid that the performance/robustness tradeoff leads to excessive control effort sensitivity function $KS(s)$ and to decrease as much as possible the input sensitivity function $SG(s)$. Adding this 4^{th} optimized parameter leads to robust high-performing as several constraints can be reached at the same time. Several industrial applications has been achieved. For instance, the robust and high performing positioning of throttle actuators for Robert Bosch GmbH (Fig. 5), and the control of a rolling skin pass for Alstom and Arcelor companies [23] (Fig. 6).

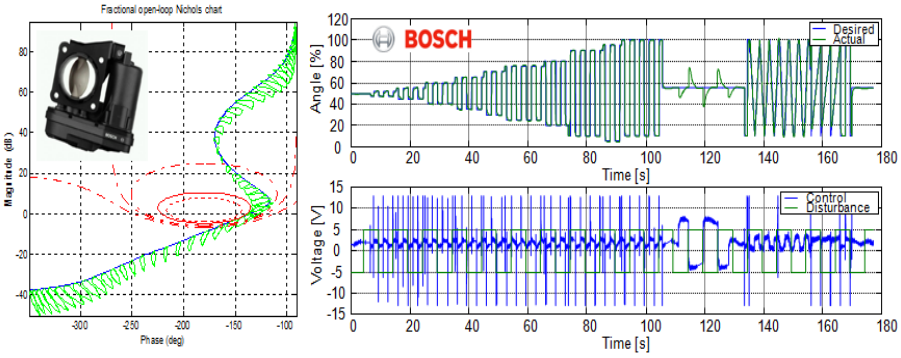

FIGURE 5. Robust design of an open-loop Nichols locus for the throttle plate of a internal combustion engine air system

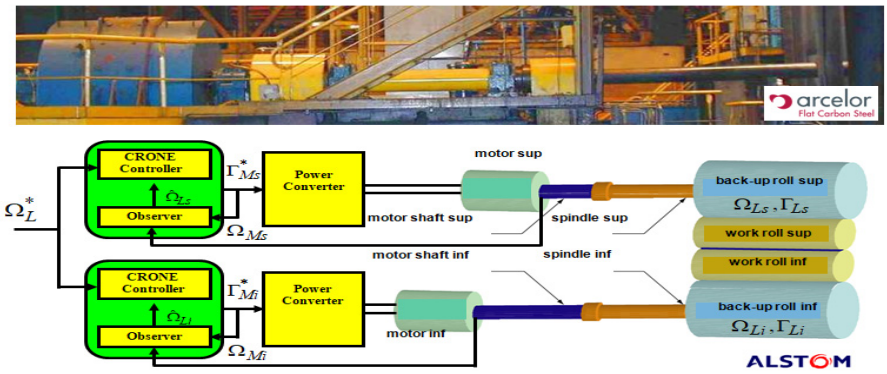

FIGURE 6. CRONE design for rolling skin pass for Alstom and Arcelor companies

In order to avoid the problem of an unfortunate choice of the arbitrary nominal plant model G_{nom} that could forbid the greatest resonant peak of

the perturbed complementary sensitivity function T to be kept small, the optimization of the nominal resonant peak M_{rd} has been proposed [4].

Well defining the frequency-domain performance constraints is highly important for designing high performing controllers. In order to make simpler the definition of these constraints, several new cost functions have been proposed to optimize simultaneously performance, for instance the closed loop bandwidth (speed of the response to the reference input and of the rejection of disturbances) and the robustness of the stability degree. The minimization of the $H\infty$ norm of $S(s)/s$ (with $S(s) = (1 + G(s)C(s)) - 1$) reveals to meet the objective as it leads to very good performance in spite of very simple constraints defined by $H\infty$ norms limiting the complementary sensitivity function $T(s) = 1 - S(s)$, the sensitivity function $S(s)$ and the input sensitivity function $C(s)S(s)$, [2].

The CRONE CSD toolbox [10], [11]for Matlab which can be download free of charge since 2010 is probably the most important development that permits the CRONE methodology to be used by many control system designers. Downloaded more than 1300 times by 1000 registered users, it permits the definition of perturbed plants, the analysis of the CSD problem, selection and initialization of the CRONE generation to be used (Fig. 7), the definition of requirements, the tuning of robust fractional order controller/open-loop, the synthesis of rational controller to be implemented and frequency and time domain simulations. Users are guided step by step all along the controller design. Many graphical interfaces and optimization algorithms allow to tune the design efficiently.

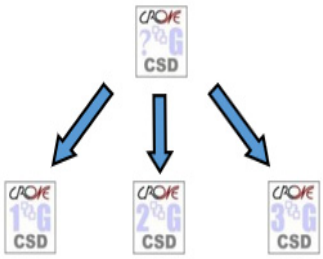

FIGURE 7. Assistance to help designers choose the CRONE methodology to be used

3. MIMO and multi-SISO CRONE control design methodologies

3.1. MIMO CRONE CSD Methodology. For MIMO systems, Four closed-loop transfer function matrices are defined:

$$\begin{aligned} S(s) = (I + G(s)C(s))^{-1} &= [S_{ij}(s)], \\ T(s) = S(s)G(s)C(s) &= [T_{ij}(s)], \\ CS(s) = C(s)S(s) &= [CS_{ij}(s)], \\ SG(s) = S(s)G(s) &= [SG_{ij}(s)]. \end{aligned} \tag{3.1}$$

For a MIMO $m \times n$ system G (n inputs, m outputs), the full MIMO CRONE CSD permits the determination of a $n \times m$ controller C that ensures the perfect decoupling of the closed-loop complementary sensitivity function T_{nom} for the nominal plant model G_{nom} [12], [14]. Thus the nominal open-loop transfer function is diagonal and is defined by:

$$\beta_{nom}(s) = G_{nom}(s) = C(s) = \begin{bmatrix} \beta_{nom11}(s) & \cdots & 0 \\ \vdots & \ddots & \vdots \\ 0 & \cdots & \beta_{nommm}(s) \end{bmatrix}. \tag{3.2}$$

Each $\beta_{nomii}(s)$ diagonal element of $\beta_{nom=(s)}$ is defined as for the third generation SISO CRONE CSD whose principle is to optimize the parameters of the nominal SISO open-loop transfer function $\beta_{nom=(s)}$ that includes $(N-+1+N+)$ band-limited complex fractional order integrators and needs to include time delay, right half-plane and/or under-damped zeros and poles related to the nominal plant. Each $\beta_{nomii}(s)$ is

$$\beta_{nomii}(s) = K_i \beta_{1i}(s) \beta_{mi}(s) \beta_{hi}(s) \beta_{Gi}(s), \tag{3.3}$$

with:

$$\beta_{1i}(s) = \left(\frac{\omega_{-N^-}}{s} + 1\right)^{n_i}, \ \beta_{hi}(s) = \frac{1}{\left(\frac{s}{\omega_{N_i^+ + 1}} + 1\right)^{n_{hi}}}, \tag{3.4}$$

$$\begin{aligned} \beta_{mi}(s) = &\sum_{k=-N_i^-}^{N_i^+} \left(\frac{1 + \frac{s}{\omega_{ik+1}}}{1 + \frac{s}{\omega_{ik}}}\right)^{\alpha_{ik}} \\ &\times \left(\mathbb{R}e_{/i}\left\{\alpha_{ik}\left(\frac{1 + \frac{s}{\omega_{ik+1}}}{1 + \frac{s}{\omega_{ik}}}\right)^{ib_{qik}}\right\}\right)^{q_{ik} sign(b_{iqik})}, \end{aligned} \tag{3.5}$$

where

$$\alpha_{i0} = \left(\frac{1 + \left(\frac{\omega_{ri}}{\omega_{i0}}\right)^2}{1 + \left(\frac{\omega_{ri}}{\omega_{i1}}\right)^2}\right)^{\frac{1}{2}} \text{ and } \alpha_{ik} = \left(\frac{\omega_{ik+1}}{\omega_{ik}}\right)^{\frac{1}{2}} \text{ and } k \neq 0. \tag{3.6}$$

n_{1i} and n_{hi} orders of β_{1i} and β_{hi} set the low frequency and high frequency behavior of $\beta_{nomii}(j\omega)$. They are respectively set from the low frequency behaviors of the i^{th} row of $G_{nom}(s)$ and from the low frequency behaviors of the i^{th} column of $P(s) = [P_{ij}(s)]$, the inverse or pseudo-inverse of $G_{nom}(s)$.

α_{ik} and b_{ik} are the real and imaginary parts of the fractional orders of band-limited integrators. ω_{ik} are their corner frequencies. The imaginary order b_{qik} and the positive integer order q_{ik} of (3.5) are determined to ensure the same open-loop phase slope as the slope ensured by an initial imaginary order b_{ik} which may have to be limited for closed-loop stability reasons [10]. For large values of b_{ik} , b_{qik} is very close to b_{ik}/b_{qik}.

N_{-i} and $N_{+}i$ are integer orders chosen different from 0 if the number of tuning parameters used for the open-loop shaping needs to be increased.

$\beta_{Gi}(s)$ is a transfer function defined from the right half plane or underdamped poles of the ith row of $G_{nom}(s)$ and of the i^{th} column of $P(s)$, and from the delays of the i^{th} column of $P(s)$.

From the given values of the other parameters, α_{i0}, b_{qi0} , q_{i0} and K_i are deduced in order to ensure a resonant frequency ω_{ri} and a and a desired resonant peak M_{rdi} of $|T_{nomii}(j\omega)|$. ω_{ri} and M_{rdi} permit the tuning of the bandwidth and of the damping of the nominal closed-loop transfer function $T_{nomii}(s)$ related to $Y_i(s)/Y_{refi}(s)$.

The parameters of all $\beta_{nomii}(s)$ are optimized together to stabilize the nominal closed-loop and to minimize the resonant peak variations of all $T_{ii}(s)$ at the time of the plant perturbation. The objective function to be minimized is defined by:

$$J = \sum_{i=1}^{m} \left(\sup_{\omega,G} |T_{ii}(j\omega)| - M_{rdi} \right). \tag{3.7}$$

The parameters to be optimized are the ω_{ik} corner frequencies, the resonant frequency ω_{iri}, the resonant peak M_{rdi}, $Y_{ri} = |\beta_{0ii}(j\omega_{ri})|$, and the orders α_{ik}, b_{qik} and q_{ik} for $i \neq 0$. When $N_i^- = N_i^+ = 0$, only 5 parameters for each $\beta_{nomii}(s)$ have to be optimized. Setting the M_{rdi} desired resonant peak for $T_{nomii}(j\omega)$ makes the Nichols plot of $\beta_{nomii}(j\omega)$ tangent to the M_{rdi} Nichols M-circle. The minimization of $J(11)$ optimizes the tangency direction in order to place the perturbed equivalent open-loop frequency response $\beta_{iieq}(j\omega)$ away from the (-π, 0dB) critical point with:

$$\beta_{iieq}(j\omega) = \frac{T_{ii}(j\omega)}{1 - T_{ii}(j\omega)}. \tag{3.8}$$

For the closed-loop performance requirement, the minimization of J is associated to 5 sets of frequency-domain inequality constraints:

$$\begin{aligned}
&\inf_{G} \ |T_{ij}(j\omega)| \geq T_{1ij}(\omega), && \inf_{G} \ |T_{ij}(j\omega)| \leq T_{uij}(\omega),\\
&\sup_{G} \ |S_{ij}(j\omega)| \leq S_{uij}(\omega) && \text{for } 1 \leq (i,j) \leq m,\\
&\sup_{G} \ |CS_{ij}(j\omega)| \leq CS_{uij}(\omega) && \text{for } 1 \leq i \leq n \text{ and for } \ 1 \leq j \leq m,\\
&\sup_{G} \ |SG_{ij}(j\omega)| \leq SG_{uij}(\omega) && \text{for } 1 \leq i \leq m \text{ and for } \ 1 \leq j \leq n. \quad (3.9)
\end{aligned}$$

As the perturbation and MIMO effects of G are taken into account without any overestimation (a set of MIMO LTI models), non-conservative (highly efficient) robust controllers can be designed. This modeling implies that a nonlinear optimization method must be used to find the optimal values of the high-level descriptive parameters of each fractional open-loop transfer function $\beta_{nomii}(s)$.

Once $\beta_{nomii}(s)$ has been optimized, the controller is obtained from

$$C(s) = P(s)\beta_{nom}(s) = \begin{bmatrix} C_{11}(s) & & C_{1m}(s) \\ & \ddots & \vdots \\ C_{n1}(s) & & C_{nm}(s) \end{bmatrix} = [C_{ij}(s)] \qquad (3.10)$$

with

$$C_{ij}(s) = P_{ij}(s)\beta_{nom_{jj}(}(s) \quad \text{for} \ \ 1 \leq i \leq n \ \ \text{and for} \quad 1 \leq j \leq m.$$

As $\beta_{nomjj}(s)$ are fractional order transfer functions, the rational transfer functions $C_{Rij}(s)$ are obtained by identifying each ideal frequency response $C_{ij}(j\omega)$computed from (3.10) by a low-order transfer function:

$$C_{R_{ij}} = \frac{B(s)}{A(s)}. \qquad (3.11)$$

where $B(s)$ and $A(s)$ are polynomials of integer degrees n_B and n_A. Many frequency-domain system identification techniques can be used. Whatever the complexity of the control problem, satisfactory values of n_B and n_A can be lower than 6 for SISO cases and lower than 10 for MIMO cases without a decrease in performance. A 2×2 robust MIMO CRONE controller has been designed for the torque and speed control of a high dynamic engine-dynamometer (D2T-FEV company) which behavior is nonlinear because of the internal combustion engine under test (Figs.8-9).

This methodology provides an efficient MIMO controller, but may be sometimes difficult to use: taking into account all the features of $P(s)$ and $G_{nom}(s)$ could be cumbersome. Thus, when a RGA analysis proves it [24], LTI square $m \times m$ MIMO uncertain plants can be controlled using decentralized (diagonal) MIMO $m \times m$ controllers.

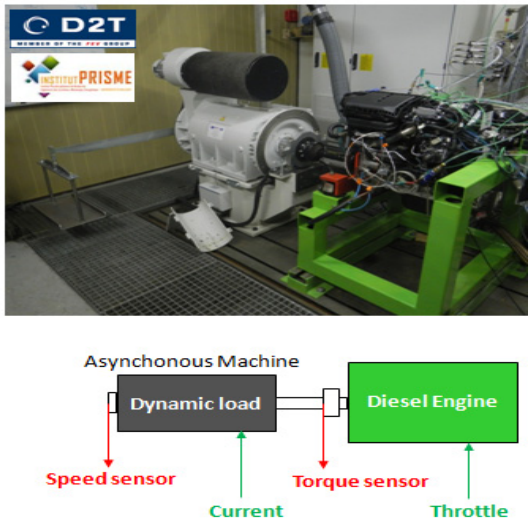

FIGURE 8. Control of Torque and speed for High Dynamic Engine-Dynamometer

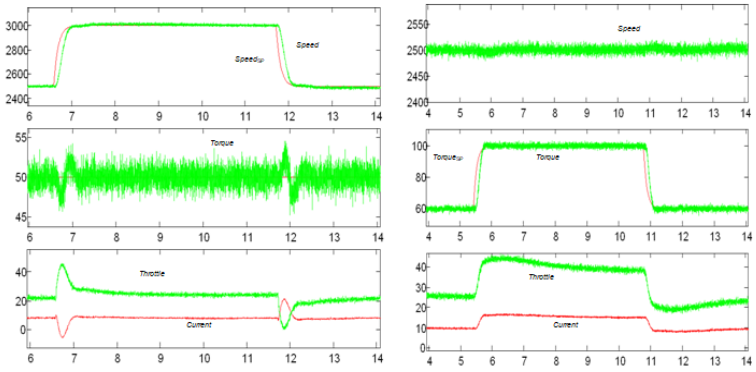

FIGURE 9. Experimental results for reference speed (left) and torque (right) variations

3.2. **MIMO design of a decentralized controller.** A decentralized controller can be obtained by choosing an arbitrary diagonal model for $G_{nom}(s)$. Nevertheless, the MIMO features of G are taken into account at the time of MIMO open-loop optimization as for instance they contribute to the resonant peak variation of all perturbed $T_{ii}(s)$, [3]. Thus, the parameters of all $\beta_{nomii}(s)$ need to be optimized at the same time. Fig. 10-11 show the application of this strategy for the control of the air-system of a

turbocharged Diesel engine, [3]. 3 control signals are used to control 2 outputs. The 3×2 controller is block-decentralized. Compared with a robust 2×2 fully decentralized CRONE controller (throttle wide open), the 3×2 controller allows reductions in both fuel consumption and NOx emission (4%) for a NEDC cycle.

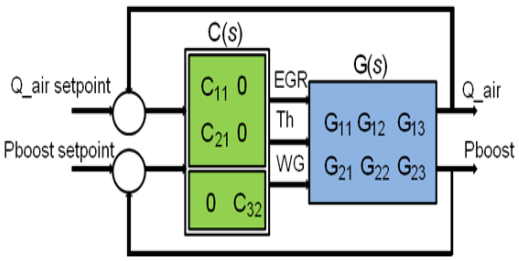

FIGURE 10. Control of fresh air flow and boost pressure of a turbocharged Diesel engine air-system

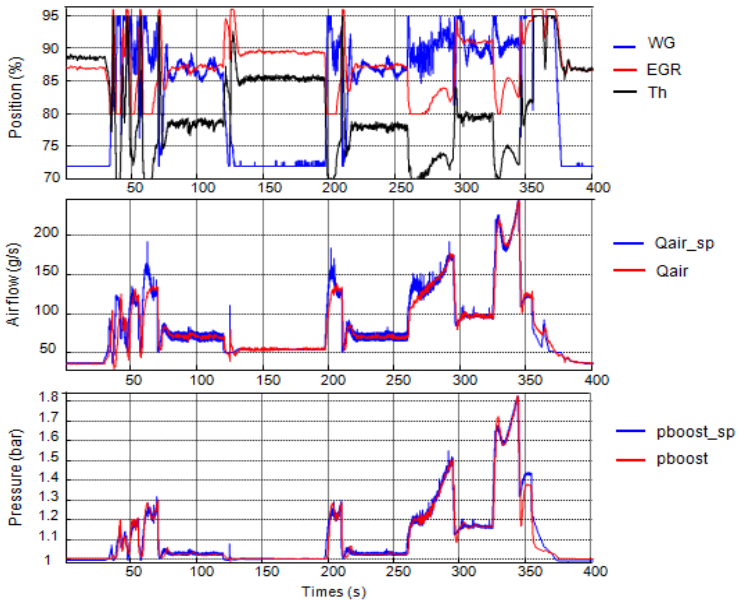

FIGURE 11. Performance comparison of 3×2 and 2×2 (Throttle wide open) CRONE MIMO controllers

3.3. **Multi-SISO design of a decentralized controller.** When the plant is diagonal dominant, the multi-SISO CRONE approach can be used to design a decentralized controller [8], [26]. This approach enables an independent tuning of each open-loop transfer function $\beta_{nomii}(s)$ (thus of each $C_i(s)$) by taking into account a diagonal nominal transfer function $G_{nomii}(s)$ and an uncertainty defined by the structured uncertainty coming from all possible values $G_{ii}(s)$ enlarged by an unstructured uncertainty computed from modulus of column off-diagonal terms $G_{ji}(s)$) (with $j \neq i$). The SISO version of the CRONE Control-System Design Toolbox [5] proposes all the functionalities to design this kind of decentralized MIMO controller.

4. Design of a decentralized controller for a MIMO refrigeration system

A non-linear MIMO Matlab/Simulink model (Fig. 12) has been built for a refrigeration system based on vapour compression [1]. This system is made of 4 components: a compressor, a condenser, an expansion valve and an evaporator. The compressor compresses the refrigerant to a high pressure and high temperature and then flows to the condenser, which is a heat exchanger where heat is rejected to the environment. The refrigerant is condensed to a liquid. The hot liquid refrigerant then passes through an expansion valve, where the refrigerant expands to a low pressure and a low temperature. The cold refrigerant then flows through the evaporator, where it absorbs heat and boils back into a vapour on its way back to the compressor. Two variables: the outlet temperature of the evaporator secondary flux $T_{e,sec,out}$ (which represent the cooling demand) and the degree of superheating T_{SH} are to be controlled by manipulating two variables: the compressor speed N and the expansion valve Av and by considering also the disturbances.

4.1. **MIMO plant analysis.** The MIMO refrigeration system needs to be analysed to know what kind of controller and control-system design methodology could be used. For this purpose, two tools can be used: Relative Gain Array Analysis (RGA) and Column Diagonal Dominance Degree (CD^3). Fig. 13 shows the decision process that indicates what kind of controller and design have to be used. Using a simplified (diagonal) nominal plant model, the full MIMO design is able to provide a decentralized controller.

In order to use the RGA, CD^3 and CRONE design tools, the previous described system needs to be linearized.

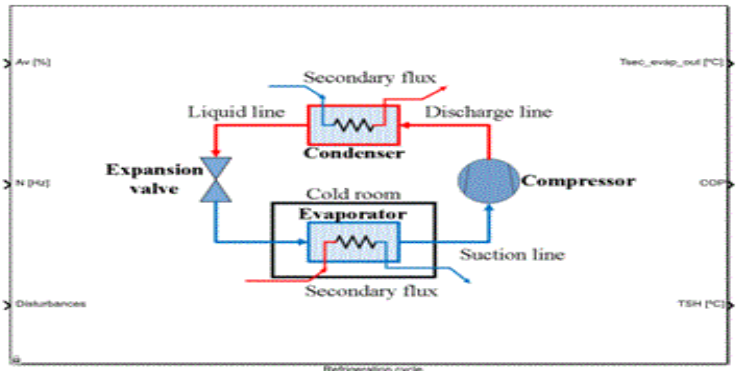

FIGURE 12. Simulink model of the refrigeration process

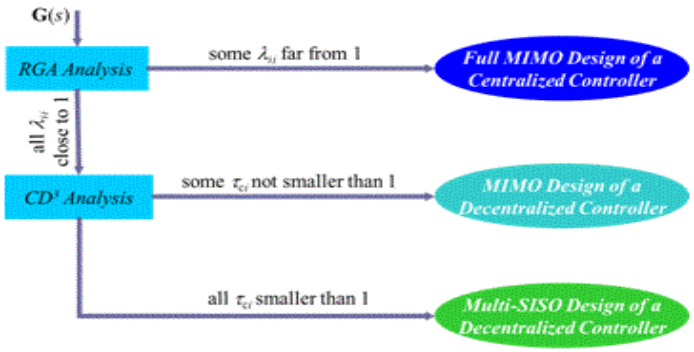

FIGURE 13. Algorithm to select Multi-SISO/MIMO design of centralized/decentralized controller

4.1.1. **System linearization.** The refrigeration system is linearized around 9 operating points (blue points in Fig. 14) chosen in the space of the controlled variables [1].

The obtained frequency responses are represented on Fig. 15. The nominal operating point is arbitrary defined by Plant # 2 located on Fig. 14. Each input-output transfer function is described by: G_{11}: from $Av(\%)$ to $T_{e,sec,out}$ (^oC); G_{12}: from N (Hz) to $T_{e,sec,out}$ $((^oC))$; G_{21}: from Av $(\%)$ to T_{SH} (^oC); G_{22}: from N (Hz) to $T_{SH}(^oC)$. From Fig. 15, we can notice variations of frequency responses due to the nonlinearities of the system. Thus, these nonlinearities will be taken into account in the controller design.

4.1.2. **RGA and CD3.** The RGA tool quantifies the relationship between an output and expresses how the output can be modified by the other

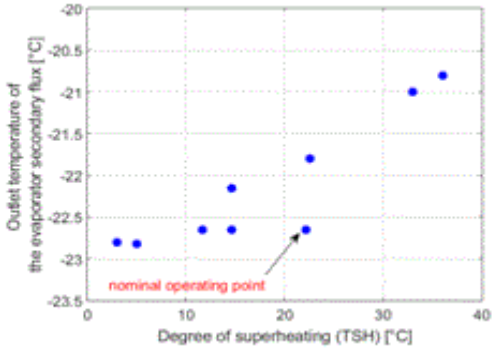

FIGURE 14. Operating points used for system linearization

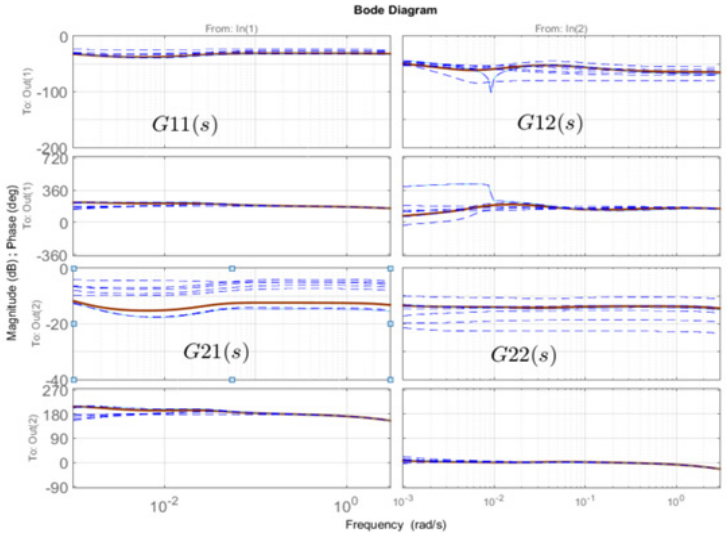

FIGURE 15. Bode diagram of nominal plant frequency response (solid brown curves) and all operating point frequency responses (blue dashed curves)

inputs. It shows the coupling level of a system and if a decentralized control could be efficient. For a given $m \times m$ plant G, the RGA matrix $\Lambda$is obtained from:

$$\Lambda(G(j\omega)) = G(j\omega)o\left(G^{-1}(j\omega)\right)^T = [\lambda_{ij}(j\omega)] \quad \text{with } i \text{ and } j \leq m. \tag{4.1}$$

For the considering MIMO system, Fig. 16 shows that for the 9 operating points, $\lambda_{11}(j\omega)$ and $\lambda_{22}(j\omega)$ are close to 1 and greater than $\lambda_{12}(j\omega)$ and

$\lambda_{21}(j\omega)$ along the studied frequency range. Thus a decentralized controller can be efficient to control the plant.

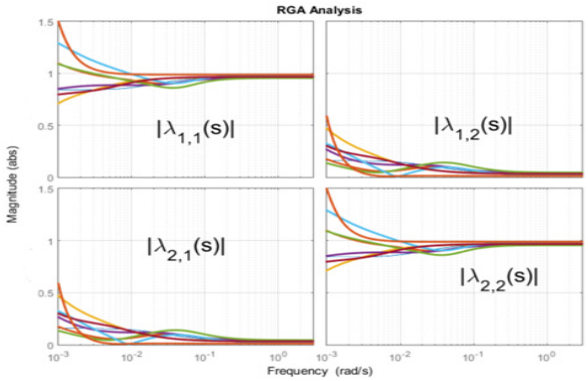

FIGURE 16. Magnitude of diagonal and off-diagonal elements of the RGA matrices of G

The CD^3 tool compares, column by column, the magnitude of each diagonal element G_{ii} of G to the sum of the magnitude of the off-diagonal elements G_{ji} with $j \neq i$. Fig. 15 shows that $|G_{22}|$ is greater than $|G_{21}|$ but $|G_{11}|$ is lower than $|G_{21}|$. Which means that, an efficient $C_2(s)$ can be designed by using the CRONE multi-SISO approach to control output y_2 of Fig. 17. At the opposite, designing $C_1(s)$ by using the multi-SISO approach would provide a conservative controller for output y_1. Nevertheless, $C_1(s)$ can be designed by using the SISO approach and by taking into account the equivalent plant $G^*_{11}(s)$ defined by $y_1/U_1(s)$ with $U_2(s) = -C_2(s)Y_2(s)$.

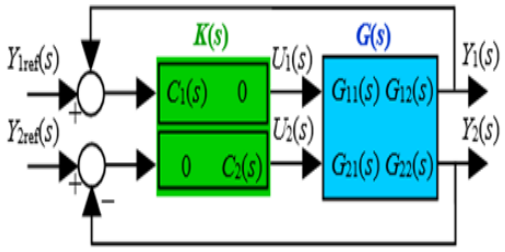

FIGURE 17. Decentralized control of a 2×2 MIMO plant

4.2. **Design of the MIMO controller.**

4.2.1. **Multi-SISO CRONE design of $C_2(s)$ controller.** Fig. 18 shows the Nichols plot of G_{22} whose uncertainty frequency domains have been enlarged by taking into account the off-diagonal elements G_{12} of G.

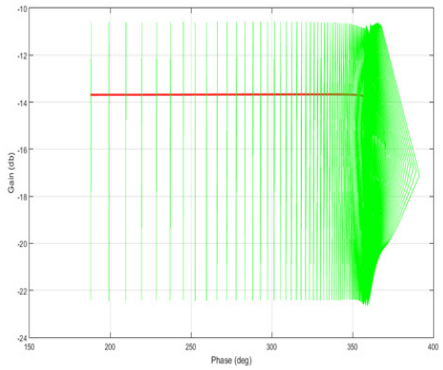

FIGURE 18. Nichols plot of $G_{22}$of G: nominal frequency responses (Red); enlarged uncertainty domains (Green)

Fig. 20 shows the frequency domain constraints that are used for the loop shaping of $\beta_{022}(s) = C_2(s)G_{022}(s)$. The desired closed-loop bandwidth is about 0.5 rad/s. In order to ensure a fast convergence of the output towards the input, T is chosen very close to $0dB$ at low frequency $(-0.1dB < T < 0.1dB)$. The sensitivity function limitation (S) is $6dB$ and the plant input sensitivity function limitation $(SG)is - 5dB$. The resonant peak limitation (T) is $2dB$. The control effort sensitivity function limitation (CS) is $25dB$. The low frequency order n_{l2} of the nominal fractional open loop open-loop transfer function $\beta_{022}(s)$ needs to be 1. To limit the control effort sensitivity at high frequency and to obtain a strictly proper controller, the high frequency order n_{h2} needs to be 2. Thus, $\beta_{022}(s)$ is defined by:

$$\beta_{022}(s) = K_2 \left(\frac{\omega_{02}}{s} + 1\right) \left(\frac{1 + \frac{s}{\omega_{12}}}{1 + \frac{s}{\omega_{02}}}\right)^{a_{02}}$$

$$\times \left(\mathbb{R}e/i \left\{ \left(a_{02} \frac{1 + \frac{s}{\omega_{12}}}{1 + \frac{s}{\omega_{02}}}\right)^{ib_2} \right\}\right)^{-q_{02} sign(b_{q02})} \frac{1}{\left(\frac{s}{\omega_{12}} + 1\right)^2}. \quad (4.2)$$

By taking into account the enlarged uncertainty of $G_{22(s)}$, the 5 optimized parameter values for β_{022} are: $Y_{r2} = 9.95$ dB; $\omega_{r2} = 0.09$ rad/s; $M_{r2} =$

0.1dB; $\omega_{02} = 0.119$ rad/s;$\omega_{12} = 2.16$ rad/s. Thus, $a_{02} = 1.08$, $b_{02} = 0.42$ and $K_2 = 2.72$. Fig. 19 presents the Nichols plot of the optimized open loop frequency response β_{022}. The final value of the cost function J is 0.12 dB and all sensitivity constraints are met. Fig. 20 shows the nominal and extreme value of the optimal sensitivity functions.

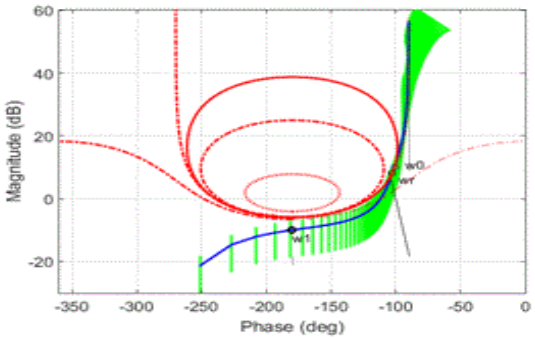

FIGURE 19. Nichols plot of β_{022} nominal frequency response (Blue); enlarged uncertainty domains (Green); 0.1 dB M-contour related to M_{T0} (Red)

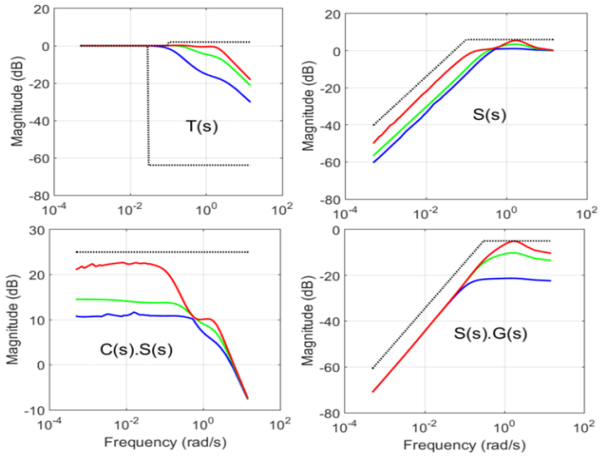

FIGURE 20. Frequency-domain constraints (—) on perturbed values of $|T(j\omega)|, |S(j\omega)|, |CS(j\omega)|and|SG(j\omega)|$

Finally, by using relation (2.4) we obtain the fractional version of $C_2(s)$ whose frequency response is fitted by an order 3 PID-like rational transfer function:

$$C_2(s) = \frac{8.063s^2 + 8.361s + 1.616}{1.253s^3 + 5.025s^2 + s}. \tag{4.3}$$

4.2.2. **SISO CRONE design of $C_1(s)$ controller.** The nominal open-loop transfer function $\beta_{011} = C_1(s)G^*_{011}(s)$ is designed by taking into account the equivalent plant $G^*_{11}(s)$ which includes the controller $C_2(s)$:

$$G^*_{11}(s) = G_{11}(s) - \frac{G_{21}(s)C_2(s)G_{12}(s)}{1 + C_2(s)G_2(s)}. \tag{4.4}$$

For β_{011}, the resonant peak limitation (T) is $4.5dB$, the sensitivity function limitation (S) is $6dB$ and the plant input sensitivity function limitation (SG) is $-19dB$. The low frequency order n_{l1} of the nominal fractional open loop open-loop transfer function $\beta_{011}(s)$ needs to be 1. To limit the control effort sensitivity at high frequency and to obtain a strictly proper controller, the high frequency order n_{h1} needs to be 2. Thus, $\beta_{011}(s)$ is defined by:

$$\beta_{022}(s) = K_2 \left(\frac{\omega_{02}}{s} + 1\right) \left(\frac{1 + \frac{s}{\omega_{12}}}{1 + \frac{s}{\omega_{02}}}\right)^{a_{02}} \times \left(\mathbb{R}e/i \left\{ \left(a_{01} \frac{1 + \frac{s}{\omega_{11}}}{1 + \frac{s}{\omega_{01}}} \right)^{ib_1} \right\} \right)^{-q_{01} sign(b_{q01})} \frac{1}{\left(\frac{s}{\omega_{11}} + 1\right)^2}. \tag{4.5}$$

The optimized parameters values are:$Y_{r1} = 8$ dB; $\omega_{r1} = 0.1$ rad/s;$M_{rd1} = 0.5dB$;$\omega_{01} = 0.009$ rad/s; ω_{11}=2 rad/s, $n_{l1} = 1$, $n_{h1} = 2$ and. Thus, $a_{01} = 1.13$, b_{01}= 0.24 and $K_1 = 40.7$. The final value of the cost function J is 0.37dB. Figs. 14-15 present the Nichols plot of the optimized open loop frequency response β_{011} and the sensitivity constraints. The PID-like rational form of $C_1(s)$ is:

$$C_1(s) = \frac{-428s^2 + 475.9s - 14.79}{42.26s^3 + 98.47s^2 + s}, \tag{4.6}$$

and the disturbances are well rejected.

4.3. **Evaluation of the designed MIMO controller.**

4.3.1. **Linear framework evaluation of the CRONE decentralized controller.** The diagram presented by Fig. 17 is used to assess the robustness and decoupling performance of the designed decentralized control-system. The 9 linear models of the plant obtained for the operating points defined by Fig. 14 are used. The simulation includes step changes in the reference signals on y_1 ($T_{e,sec,out}$) and y_2 (T_{SH}) at different times and at the same time (Fig. 24). Fig. 24 shows that plant outputs are both stable

and damped: overshoot $\leq 20\%$. Furthermore, coupling disturbances are well rejected.

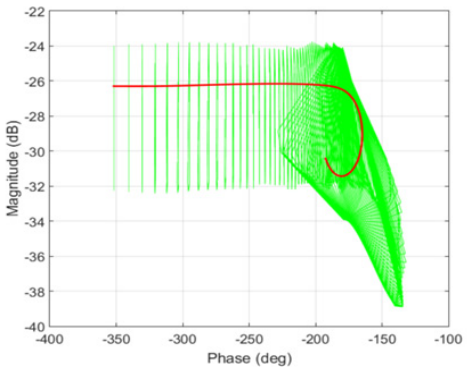

FIGURE 21. Nichols plot of G_{11}^{*}: nominal frequency response (Red); uncertainty domains (Green)

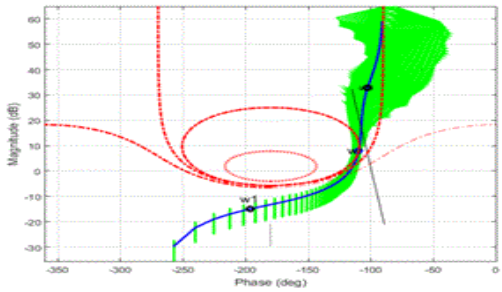

FIGURE 22. Nichols plot of β_{011} nominal frequency response (Blue); uncertainty domains (Green); 0.5 dB M-contour related to M_{T0} (Red))

4.3.2. **Final evaluation of the CRONE decentralized controller and comparison with two reference controllers.** A standard simulation have been performed using the full nonlinear model. This simulation, includes step changes in the input signals references on $T_{e,sec,out}$ and T_{SH} and in the most important disturbances: the inlet temperature of the evaporator secondary flux $T_{e,sec,in}$ and the inlet temperature of the condenser secondary flux $T_{e,sec,in}$. A sampling time of 1 second is considered. Fig. 25 presents the results of the standard simulation using the decentralized CRONE controller defined from (4.3) and (4.6).

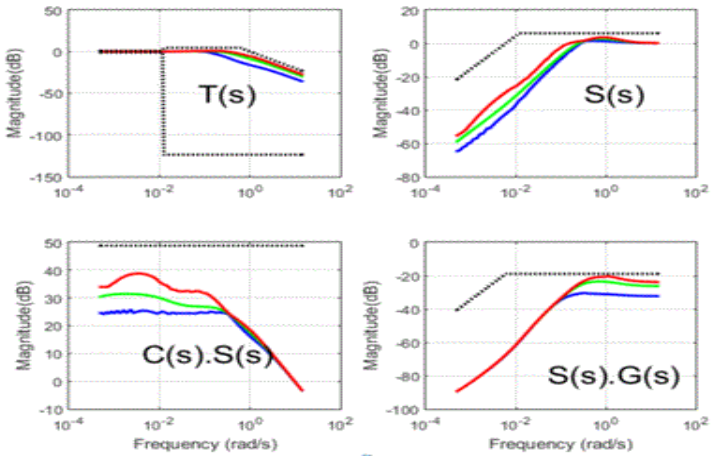

FIGURE 23. Frequency-domain constraints (—) on perturbed values of $|T(j\omega)|, |S(j\omega)|, |CS(j\omega)|and|SG(j\omega)|$

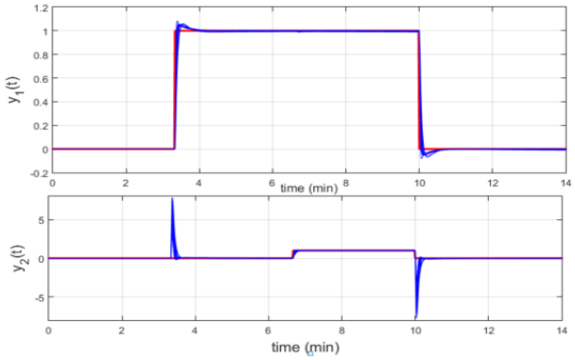

FIGURE 24. Time simulation with the decentralized controller for 9 linear models of the MIMO plant

The CRONE controller is also compared with the default PID decentralized controller given by the Benchmark PID 2018. CRONE controller provides good response of $T_{e,sec,out}$ and T_{SH} for a fairly close control effort level. Plant outputs are stable and well damped: the percentage overshoots are always less than 20% with the respect to the input references and a settling time less than 30s. Moreover, it is important to observe that the plant outputs are decoupled and the disturbances are well rejected.

Furthermore, Benchmark PID 2018 proposes a set of absolute and relative indexes to compare new designed controllers to a default PID controller. An improved MIMO controller is also proposed. For all relative indexes and

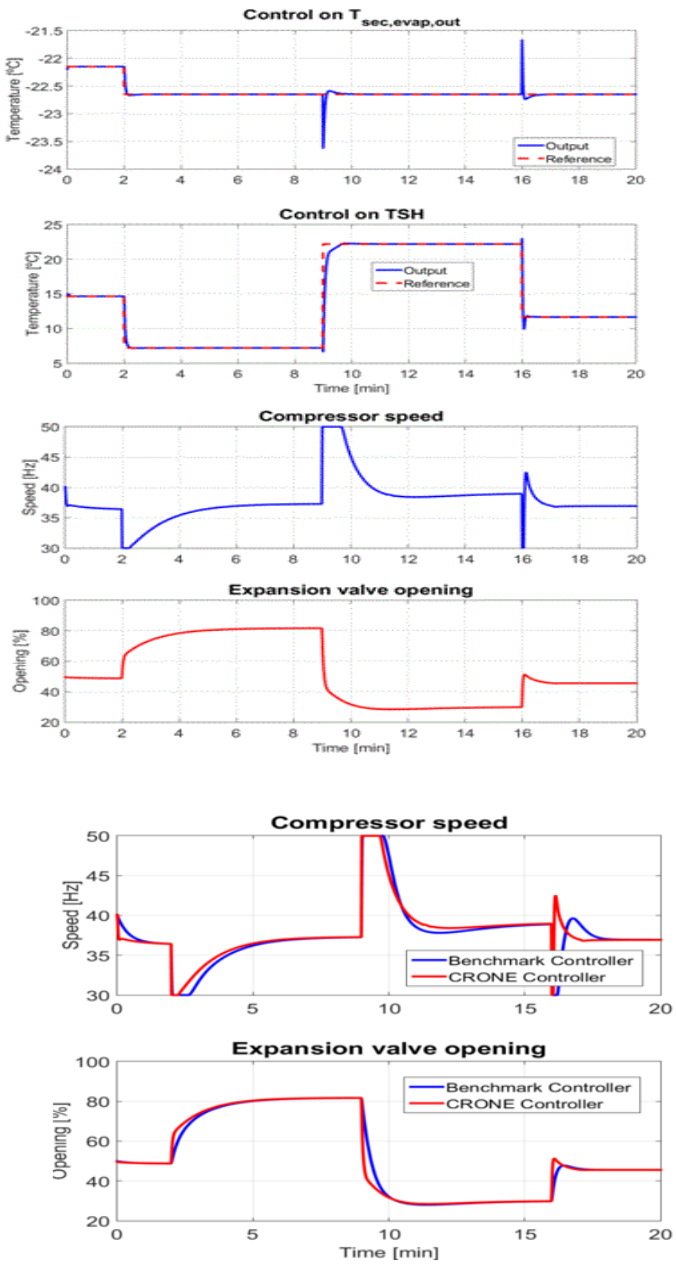

FIGURE 25. Simulation results with the MIMO Refrigeration Control System: controlled and manipulated variables

globally, the table in Fig. 26 permits the comparison of the MIMO CRONE

controller and of the improved Benchmark's MIMO controller to the default PID controller. It shows that the relative indices quantifying the error signals ("E") for the CRONE controller are twice better than those of the improved MIMO. Relative indices quantifying the control signals ("U") shows that the control energy is almost the same for the 3 controllers.

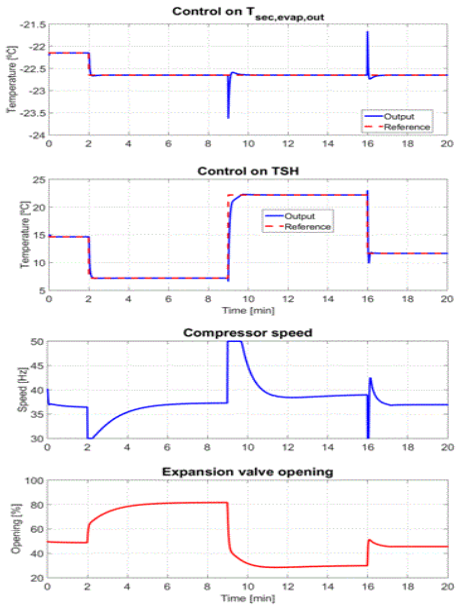

Index	CRONE MIMO controller	Benchmark's MIMO controller
$RIAE_1(C_2, C_1)$	0.28196	0.3511
$RIAE_2(C_2, C_1)$	0.2918	0.4458
$RITAE_1(C_2, C_1, t_{c1}, t_{s1})$	0.21776	1.6104
$RITAE_2(C_2, C_1, t_{c2}, t_{s2})$	0.09181	0.1830
$RITAE_2(C_2, C_1, t_{c3}, t_{s3})$	0.13766	0.3196
$RITAE_2(C_2, C_1, t_{c4}, t_{s4})$	0.065014	0.1280
$RIAVU_1(C_2, C_1)$	1.0567	1.1283
$RIAVU_2(C_2, C_1)$	1.1143	1.3739
$J(C_2, C_1)$	0.2751	0.68209

FIGURE 26. Quantitative comparison of MIMO controllers with the default Benchmark PID

5. Conclusion

The roots of the CRONE control methodology are old and for 25 years, it has been developed in order to make it bot high performing and simple to be used by designers. Initially devoted to SISO systems, the CRONE methodology is now extended to MIMO systems. Even if most of the time, decentralized controllers are designed without taking into account the coupling effects of MIMO plants, this paper shows that the coupling effects can be taken into account explicitly and simply by using an extension of the 3rd generation of the SISO CRONE methodologies. The model of a 2 inputs 2 outputs MIMO and nonlinear refrigeration system provided as a benchmark for the PID 2018 conference has been used to illustrate the proposed design approach. The 2 terms of the controller are successively designed using the multi-SISO approach and then the SISO CRONE CSD approach. Good control performances of the proposed controller have been demonstrated in simulation.

References

[1] G. Bejarano, JA. Alfaya, D. Rodriguez, MG. Ortega, F. Morilla, Benchmark for PID control of Refrigeration Systems based on Vapour Compression. *IFAC PapersOnLine*. **51**, No 4 (2018), 497–502.

[2] B. Feytout, P. Lanusse, J. Sabatier, S. Gracia, Robust CRONE design for a variable ratio planetary gearing in a variable speed wind turbine. *Asian. J. Control* **15**, No 3 (2013), 806–818.

[3] A. Lamara, G. Colin, P. Lanusse, Y. Chamaillard, A. Charlet, Decentralized robust control-system for a non-square MIMO system, the air-path of a turbocharged Diesel engine. *IFAC Proc.* **45**, No 30 (2012), 130–137.

[4] A. Lamara, P. Lanusse, D. Nelson-Gruel, Y. Chamaillard, A. Lesobre, A. Oustaloup, Additional optimization parameter for a simplified design of third generation CRONE controllers. In: *The 10th IEEE/ASME International Conference on Mechatronic and Embedded Systems and Applications*, Ancona, Italy (2014).

[5] P. Lanusse, A. Oustaloup, C. Ceyral, M. Nouillant, Optimal CRONE control of a tractor hich system. *IFAC Proc.* **25**, No 13 (1992), 301–307.

[6] P. Lanusse, A. Oustaloup, B. Mathieu, Third generation CRONE control. In: *IEEE/SMC'93 Conference*, Le Touquet, France (1993).

[7] P. Lanusse, *De la commande CRONE de première génération à la commande CRONE de troisième generation*. PhD Thesis, Bordeaux I University, France (1994).

[8] P. Lanusse, A. Oustaloup, D. Sutter, Multi-scalar CRONE control of multivariable plants. In: *WAC'96-ISIAC Symphosia*, Montpellier, France (1996).
[9] P. Lanusse, A. Oustaloup, B. Mathieu, Robust control of LTI square MIMO plants using two CRONE control design approaches. *IFAC. Proc.* **33**, No 14 (2000), 379–384.
[10] P. Lanusse, *CRONE Control System Design, a CRONE toolbox for Matlab*, http://www.ims-bordeaux.fr/CRONE/toolbox (2010).
[11] P. Lanusse, R. Malti, P. Melchior, Crone control system design toolbox for the control engineering community: tutorial and a case study. *Phil. Trans. Roy. Soc.* **371**, No 1990 (2013), 120–149; DOI: 10.1098/rsta.2012.0149.
[12] P. Lanusse, D. Nelson-Gruel, A. Lamara, Toward a CRONE toolbox for the design of full MIMO controllers. In: *Intern. Conf. on Fractional Differentiation and its Applications*, Novi Sad, Serbia (2016).
[13] PSV. Nataraj, S. Tharewal, On fractional-order QFT controllers. *J. Dyn. Sys., Meas., Control* **129**, No 2 (2007), 212–218.
[14] D. Nelson-Gruel, P. Lanusse, A. Oustaloup, Decentralized CRONE control of mxn multivariable system with time-delay. In: *3nd IFAC Workshop on "Fractional Differentiation and its Applications" (FDA'08)*, Ankara (2008).
[15] A. Oustaloup, *Systèmes asservis linéaires d'ordre fractionnaire*. Masson, Paris (1983).
[16] A. Oustaloup, *La commande CRONE*. Hermes Editor, Paris (1991).
[17] A. Oustaloup, A. Ballouk, P. Lanusse, Synthesis of a narrow band template based on complex non integer derivation. In: *IMACS Symposium "Modelling and control of technological systems"*, Lille, France (1991).
[18] A. Oustaloup, P. Lanusse, A. Elyagoubi, Synthesis of a wide band template based on the Viète's functions. In: *IMACS Symposium "Modelling and control of technological systems"*, Lille, France(1991).
[19] A. Oustaloup, P. Lanusse, Commande CRONE optimale (Optimal CRONE control). In: *Meeting of the CNRS French Automatic Control Community*, Grenoble, France (1992).
[20] A. Oustaloup, B. Mathieu, P. Lanusse, The CRONE control of resonant plants: Application to a flexible transmission. *Euro. J. Control* **1**, No 2 (1995), 113–121.
[21] A. Oustaloup, F. Levron, B. Mathieu, F. Nanot, Frequency-band complex noninteger differentiator: characterization and synthesis. *IEEE. Trans. Circuits. Sys.* **47**, No 1 (2000), 25–39.
[22] I. Petras, The fractional-order controllers: Methods for their synthesis and application. *J. Elec. Eng.* **50**, No 9 (1999), 284–288.

[23] S. Poullain, P. Latteux, JL. Thomas, J. Sabatier, A. Oustaloup, Robust speed control of a low damped electromechanical system based on CRONE control: Application to a four mass experimental test bench. *Non. Dyn.* **50**, No 1 (2004), 383–400.

[24] J. Sabatier, P. Lanusse, P. Melchior, A. Oustaloup, *Fractional Order Differentation and Robust Control Design*. Springer Academic edition, (2015).

[25] P. Shah, S. Agashar, Review of fractional PID controller. *Mechatronics* **38** (2016), 29–41.

[26] D. Sutter, *La commande CRONE multiscalaire: application à des systèmes mécaniques articulés*. PhD Thesis, Bordeaux I University, France (1997).

[1] *Bordeaux INP, IMS CNRS UMR 5218, FRANCE*
Université de Bordeaux, IMS CNRS UMR 5218, FRANCE
e-mail: patrick.lanusse@ims-bordeaux.fr *Received: March 10, 2019*

[2] *Bordeaux INP, IMS CNRS UMR 5218, FRANCE*
Université de Bordeaux, IMS CNRS UMR 5218, FRANCE
e-mail: tari.massinissa@gmail.com

Please cite to this paper as published in:
Fract. Calc. Appl. Anal., Vol. **22**, No 5 (2019), pp. 1177-1202
DOI: 10.1515/fca-2019-0063; at https://www.degruyter.com/view/j/fca.